Journal of Scientific Research & Reports
5(2): 120-131, 2015; Article no.JSRR.2015.079
ISSN: 2320-0227

SCIENCEDOMAIN *international*
www.sciencedomain.org

The Structural Design of Six-Axis Force/Torque Sensor Using Virtual Prototyping Technique

Hilman Syaeful Alam[1*], Demi Soetraprawata[1] and Bahrudin[1]

[1]Technical Implementation Unit for Instrumentation Development, Indonesian Institute of Sciences, Jl. Sangkuriang Komp. LIPI Gd. 30, Bandung, 40135, Indonesia.

Authors' contributions

This work was carried out in collaboration between all authors. Author HSA designed the study, wrote the protocol, and wrote the first draft of the manuscript. Author DS managed the literature searches and analyses the simulation results and Bahrudin conducted the finite element simulation. All authors read and approved the final manuscript.

Article Information

DOI: 10.9734/JSRR/2015/14921
Editor(s):
(1) Luigi dell'Olio, School of Civil Engineering, Channels and Ports, University of Cantabria, Cantabria, Spain.
Reviewers:
(1) Anonymous, The University of Michigan, USA.
(2) Wang Yong, Mechinical School, Tianjin University Of Commerce, China.
(3) Anonymous, Higher Technical Institute, Technical University of Lisbon, Portugal.
Complete Peer review History: http://www.sciencedomain.org/review-history.php?iid=748&id=22&aid=7195

Original Research Article

Received 28th October 2014
Accepted 18th November 2014
Published 15th December 2014

ABSTRACT

The design of a six-axis F/T sensor is an important and challenging research to produce a sensor that is able to measure simultaneously the six-component force and torque accurately and efficiently. The structural design is one of the key issues to be considered to improve the performances of the sensor that cross coupling is the most important factor regarding a sensor quality. The purpose of this study is to design a six-axis F/T sensor that has a novel and compact design, has a low coupling error and can meet the design criteria such as mechanical strength, stiffness, and reliability in the receiving load. Virtual prototyping technique is applied with the aim to shorten the time and reduce the manufacturing cost of the physical prototypes. In this study, the six-axis F/T sensor is designed using four cross beam symmetrically that is able to measure three axial forces (Fx, Fy, Fz) and three axial moments (Mx, My, Mz). Based on the structural integrity evaluation, the structure of the sensor will certainly secure to the plastic failure of materials because it is still in the area of the material elasticity. Then based on the simulation results of the strain, the highest cross-coupling errors is -1.67% which is relatively small compared to the principal coupling error. Therefore, the design of six-axis F/T sensor using virtual prototyping

**Corresponding author: Email: hilman.syaeful.alam@lipi.go.id;*

technique is able to show satisfactory results and can be used as a guideline for manufacturing the physical prototype.

Keywords: Six axis F/T sensor; virtual prototyping; coupling error.

1. INTRODUCTION

Multi-axial force/torque (F/T) sensors have recently received attention in various engineering fields such as the nuclear power plant, ship building, voyage and aviation, aerospace, chemical engineering, national defense, medicine, biology and micro-mechanical system 1. Numerous studies of the multi-axial F/T sensors have been carried out for a variety of applications, such as: force sensing tools for disassembly operations 2, force control of polishing machine for vehicle body 3, sensor for biomedical and robotic devices [4,5 micro-manipulation 6, lumbar inter-body load measurements 7, hand manipulator for retinal surgery 8, and wind tunnel balance 9. A six-axis F/T sensor is one of the multi-axial sensor which is able to simultaneously measure all the force and torque components of an arbitrary six-component force system, i.e. three axial forces (Fx, Fy, Fz) and three axial moments (Mx, My, Mz) 910.

With the ability of measuring three force components and three torque components, the six-axis F/T sensor is one kind of the most important and challenging sensors, that can measure six-component force/torque accurately and efficiently. The structural design is one of the key issues to be considered since the improvements on the performances of the sensor, such as the isotropy, sensitivity, stiffness, stress coupling, dynamic performance, economical etc., can be achieved with the selection of suitable structural parameters 1112]. Several researchers have developed a six-axis F/T sensor with various types and design structures, such as: parallel mechanism 110, microstructure based on piezo resistive device 6, crossbeam 913, based E-type membranes 10, Stewart platform-based 11 and parallel spoke piezoelectric 14. Some designs of six-axis F/T sensor have achieved a good characteristic such as the decreasing of coupling error but it still involve the complicated structure and specific material, so that made them heavy and expensive.

The cross coupling is the most important factor regarding sensor quality in developing the six-axis F/T sensor which is generally ranging from 3 to 37%. The cross coupling is conceptually defined as the ratio of unfavorable signal to the intended signal at a given bridge circuit according to pure force components. For example, suppose that a circuit output signal which is intended to measure force F_x , also response to moment M_y . In this case, cross coupling is the ratio of the output signal under the maximum M_y (unfavorable signal) to that under the maximum F_x (intended signal) 13. Some studies on multi-axis F/T sensors have reported low coupling error (CE), Yingkun et al. 1 produces the CE of 8.5%, Liang et al. 10 produces the CE of 1.6%, and Kang et al. 13 produces the CE of 2.5%. In order to minimize coupling errors, the location of strain gauges on the sensor structure must be search and determined.

One of the techniques that can be applied to determine the characteristics of a solid structure (such as deformation, stress, and strain) is a virtual prototyping. This technique can help the realization process of a product by creating the model geometry in 3-dimensional (3D) and simulate its performance before physical prototypes are made, so it can reduce the manufacturing cost of the physical prototypes, can shorten the time and reduce the cost of the product development 1. Because of these advantages, then at the some previous research, a virtual prototyping technique has been applied for designing and developing products in various applications, such as: traction mechanism of heavy machinery 15, bridge construction 16, predicted emission 17, footwear 18, injection moulding 19, and so on. In this study, a six-axis F/T sensor is designed using virtual prototyping techniques based on finite element method (FEM) to produce a virtual prototype which is able to simultaneously measure three axial forces (Fx, Fy, Fz) and three axial moments (Mx, My, Mz) with a novel and compact design, a low coupling error and a safety factor that satisfies the requirements.

2. MATERIALS AND METHODS

2.1 Design Criteria of Six Axis F/T Sensor

According to Kang et al. 13, If the six-axis F/T sensor having loading, $\vec{F} = [F_x, F_y, F_z, M_x, M_y, M_z]^T$, on the structure in the elastic region, then the resultant strain generated in n Wheatstone bridges can be written as a $n \times 1$ strain output vector, $\vec{S}$. Therefore, the relationship between the load vector and the strain output vector can be calculated using the following equation:

$$\vec{S} = [C]\vec{F} \qquad (1)$$

where $[C]$ is an $n \times 6$ strain compliance matrix whose element C_{ij} represents the strain contribution at bridge circuit i due to a unit pure load j (there are 6 directions of measurement, so that $n = 6$).

When the maximum pure load for $x$direction is applied ($\vec{F}_1 = [F_x^{max} \quad 0 \quad 0 \quad 0 \quad 0 \quad 0]^T$), the corresponding strain output vector is: $\vec{S}_1 = [S_{11} \quad S_{21} \quad \dots \quad S_{61}] = [C]\vec{F}_1 = F_x^{max} \times [C_{11} \quad C_{21} \quad \dots \quad C_{61}]^T$ and only C_{ij} for $j = 1$ becomes active. This relationship for the other maximum pure load components can be written as follows:

$$\begin{aligned}
\vec{S}_2 &= F_y^{max} \times [C_{12} \quad C_{22} \quad \dots \quad C_{62}]^T \\
\vec{S}_3 &= F_z^{max} \times [C_{13} \quad C_{23} \quad \dots \quad C_{63}]^T \\
\vec{S}_4 &= M_x^{max} \times [C_{14} \quad C_{24} \quad \dots \quad C_{64}]^T \qquad (2) \\
\vec{S}_5 &= M_y^{max} \times [C_{15} \quad C_{25} \quad \dots \quad C_{65}]^T \\
\vec{S}_6 &= M_z^{max} \times [C_{16} \quad C_{26} \quad \dots \quad C_{66}]^T
\end{aligned}$$

The strain matrix, S, can be defined by combining six $\vec{S}_j$ column vector using the following equation:

$$SS = [S_{ij}] = \begin{bmatrix} S_{11} & S_{12} & S_{13} & S_{14} & S_{15} & S_{16} \\ S_{21} & S_{22} & S_{23} & S_{24} & S_{25} & S_{26} \\ S_{31} & S_{32} & S_{33} & S_{34} & S_{35} & S_{36} \\ S_{41} & S_{42} & S_{43} & S_{44} & S_{45} & S_{46} \\ S_{51} & S_{52} & S_{53} & S_{54} & S_{55} & S_{56} \\ S_{61} & S_{62} & S_{63} & S_{64} & S_{65} & S_{66} \end{bmatrix} \qquad (3)$$

From eq. (3), F/T sensor is completely decoupled if the strain matrix is a diagonal matrix with all zero of off-diagonal values. In contrast, when one bridge circuit responds to more than one of the component loading, non zero S_{ij} ($i \neq j$) will appear and will sacrifice some range portion of the$i$-th bridge circuit and cause a reduction in the resolution of the measurement on the load component i , where the resolution will be decreased in proportion to the increase in the ratio of S_{ij} to S_{ii}. Therefore, the cross coupling error as the design criteria of a six-axis F/T sensor can be calculated using the following equation:

$$(CC)_{ij} = \frac{S_{ij}}{S_{ii}} \qquad (4)$$

where i=1,...,6 dan $i \neq j$

2.2 Structure and Strain Gauge Configurations

The structure of six axis F/T sensor can be seen in Fig. 1. Six axis F/T sensor is designed using four cross beam (1-4), where in each beam, it is mounted six strain gauge with a certain configuration therefore the total strain gauge attached is 24 pieces. One of the four sides of the beam is connected to the plate (7) that blends with outer ring of the sensor structure.

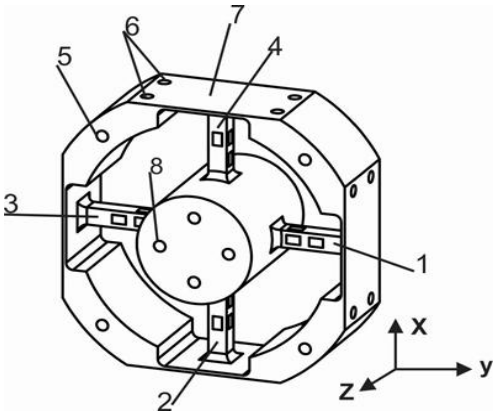

Fig. 1. Structure of the six axis F/T sensor

On the outer ring, the bolt hole is made as a fixture to hold the sensor when the load is applied on the sensor. Plate connector between the beam and the outer ring is designed thinner than the outer dimensions of the ring, to give the effect of a spring so that it will increase the flexural deformation and increase of sensitivity of the horizontal lateral forces (Fx and Fy). While the other side of the beam is connected to the

cylinder block (8) which has four bolt holes for mounting fixture loading where force or moment will be applied. The materials of six-axis F/T sensor is made of AISI 4340 steel that has a high tensile strength at 745 MPa, Yield strength of 470 Mpa, elastic modulus of between 190 to 210 GPa, and Poisson's ratio of between 0.27 to 0.30.

The strain gauge location has a configuration as shown in Fig. 2(a), where the strain gauge distance to the center of the cylinder block (X1 and X2) can be seen in Fig. 2(b). Six axis F/T sensor is designed to be able to measure a 3-way force (F_x, F_y, F_z) and 3-way moments (M_x, M_y, M_z) using six pieces of bridge circuits, where each circuit consists of 4 pieces of strain gauge. The output strain of each load component is calculated using the following equation:

$$S_{Fx} = \frac{\varepsilon_1 - \varepsilon_2 + \varepsilon_3 - \varepsilon_4}{4}$$

$$S_{Fy} = \frac{\varepsilon_{G5} - \varepsilon_{G6} + \varepsilon_{G7} - \varepsilon_{G8}}{4}$$

$$S_{Fz} = \frac{\varepsilon_{G9} - \varepsilon_{G10} + \varepsilon_{G11} - \varepsilon_{G12}}{4} \quad (5)$$

$$S_{Mx} = \frac{\varepsilon_{G13} - \varepsilon_{G14} + \varepsilon_{G15} - \varepsilon_{G16}}{4}$$

$$S_{My} = \frac{\varepsilon_{G17} - \varepsilon_{G18} + \varepsilon_{G19} - \varepsilon_{G20}}{4}$$

$$S_{Mz} = \frac{\varepsilon_{G21} - \varepsilon_{G22} + \varepsilon_{G23} - \varepsilon_{G24}}{4}$$

2.3 Virtual Prototyping

The design of a six-axis F / T sensor using virtual prototyping technique is based on the finite element method. The basis of the finite element is to divide the solids into small elements that are finite in number, therefore the reaction due to the load can be calculated on the given boundary conditions. From these elements, it can be arranged the matrix equations that can be solved numerically. By the calculations of the inverse matrix, it will be obtained the matrix equation for the single element and the total matrix that is assemblage from the matrix elements 2021. In 3D finite element, one type of element which is widely applied for the geometry of complex structures is a tetrahedral element. Fig. 3(a) shows the discretization of 3D solid structure that is divided into a set of finite number of tetrahedral elements, whereas in Fig. 3(b) tetrahedral element has four surfaces and four nodal points that relative to the coordinate plane. Each nodal has three degrees of freedom (DoF) therefore the total DoF in a tetrahedral element is 12.

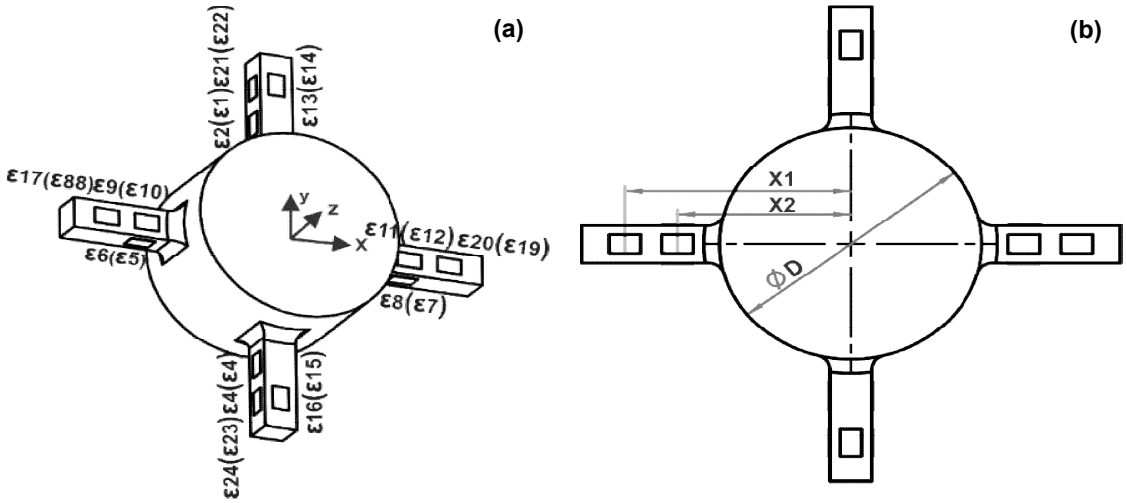

Fig. 1(a). Strain gauge configuration (b) strain gauge distance to the center of the cylinder block

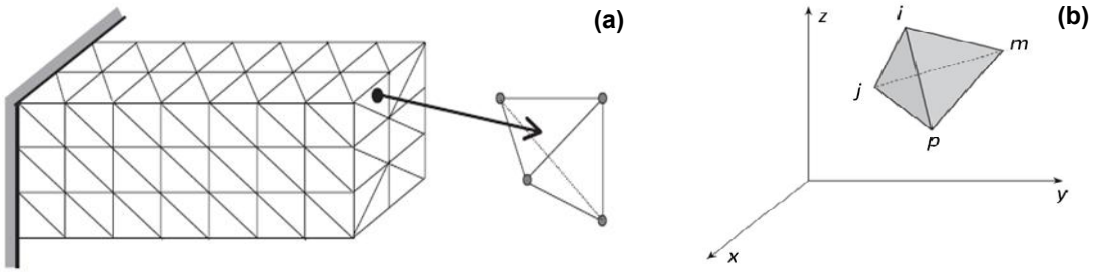

Fig. 2(a). Discretization of solid structure 20, (b) the nodal coordinates of tetrahedral element 21

According to Zienkiewicz and Taylor 21, the general form of the equation in solving the stress and strain problems for continuum structures based on the calculation of matrix elements in the elastic region is as follows:

$$\sigma = \begin{Bmatrix} \sigma_x \\ \sigma_y \\ \sigma_z \\ \tau_{xy} \\ \tau_{yz} \\ \tau_{zx} \end{Bmatrix} = \mathbf{D}\varepsilon \tag{6}$$

where $\mathbf{D}$ is the elasticity matrix based on the material's elastic constants E and Poisson's ratio υ, which can be calculated by the equation:

$$\mathbf{D} = \frac{E}{(1+\upsilon)(1-\upsilon)} \begin{bmatrix} 1-\upsilon & \upsilon & \upsilon & 0 & 0 & 0 \\ & 1-\upsilon & \upsilon & 0 & 0 & 0 \\ & & 1-\upsilon & 0 & 0 & 0 \\ & & & (1-2\upsilon)/2 & 0 & 0 \\ & & & & (1-2\upsilon)/2 & 0 \\ Sym. & & & & & (1-2\upsilon)/2 \end{bmatrix} \tag{7}$$

Strain matrix consists of six components of strain in the three-dimensional analysis, can be calculated:

$$\varepsilon = \begin{Bmatrix} \varepsilon_x \\ \varepsilon_y \\ \varepsilon_z \\ \gamma_{xy} \\ \gamma_{yz} \\ \gamma_{zx} \end{Bmatrix} = \left[\mathbf{B}_i, \mathbf{B}_j, \mathbf{B}_m, \mathbf{B}_p\right]\mathbf{a}^e \tag{8}$$

where the displacement element is defined as the twelve components of the displacement at the nodal point:

$$\mathbf{a}^e = \begin{Bmatrix} \mathrm{a}_i \\ \mathrm{a}_j \\ \mathrm{a}_m \\ \mathrm{a}_p \end{Bmatrix} \tag{9}$$

with,

$$\mathbf{B}_i = \frac{1}{6V} \begin{bmatrix} b_i, & 0 & 0 \\ 0 & c_i, & 0 \\ 0 & 0 & d_i, \\ d_i, & b_i, & 0 \\ 0 & c_i, & c_i, \\ d_i, & 0 & b_i, \end{bmatrix} \tag{10}$$

where the other **B** matrix can be obtained by substituting the appropriate sub-script.

In this study, the finite element simulation was performed using ANSYS to analyze the strain and the structural integrity of the sensor structure. The first stage in the simulation is modeling the 3D geometry of the component that is modeled for the analysis of homogeneous and linear elastic with AISI 4340 material. The next stage is the discretization or meshing of the solid. The process of meshing was performed using 3D tetrahedral element type. After meshing, the next step is to determine the boundary conditions and loading, therefore the simulation can proceed to the calculation stage and reporting of the desired results, such as strain, deformation and stress.

The imposition of loads (F_x, F_y, F_z) was performed well for the direction of tension and compression loads ranging from 20% up to a maximum load of 2000 N and for a moment (M_x, M_y, M_z) was performed on the CW and CCW direction ranging from 20% load to a maximum moment of 80 Nm which each force and moment is applied stepwise by dividing the whole load range into ten increments. The strain analysis was performed to find the location of the strain gauge (X1 and X2 in Fig. 2(b)) on the cross beam structure which is based on the value of a low cross coupling errors. The structural integrity of the sensor is based on the plastic collapse criterion or the ratio of equivalent stress to the yield strength of the material that should be more than 1.0.

3. RESULTS AND DISCUSSION

The results of geometric modeling of six-axis F/T sensor in 3D using ANSYS design modeler can be seen in Fig. 4(a). The structure of the sensor is designed using 4 cross beam symmetrically to generate strain measurements that have low cross coupling errors. Then based on the stage in the finite element simulation, the model is divided into small elements through the process of meshing or discretization models. The results of discretization 3D model of a six-axis F/T sensor can be seen in Fig. 4(b). Types of elements that used in the finite element simulation is tetrahedral element, which consists of 33,426 elements and 58,539 nodes.

After going through the iterations and calculations, the virtual prototyping simulation results, such as deformation, equivalent stress, safety factor and the strain can be determined for each segment of the six-axis F/T sensor. Fig. 5(a) shows the magnitude of the deformation due to the maximum loading F_x of 2000 N. The maximum amount of deformation in the direction of the X axis is 0.0384 mm, where the locations of maximum deformation is found in the red colored on the structure, while on the pedestal (bolt holes) the deformation does not occur, because the boundary condition used is fixed restraint. The Von Mises stress on the structure due to F_x can be seen in Fig. 5(b), where the maximum stress is 166.72 MPa, located on the flexible plate of the outer ring. The deformation, stress and safety factor to the yield for all loading ($F_x, F_y, F_z, M_x, M_y, M_z$) can be seen in Table 1. Based on the structural integrity of the sensor for all loading, the maximum equivalent stress occurs in moment M_x of 307.30 MPa, however the minimum safety factor is still 53% greater than the yield strength of the material, Therefore the structure of the six-axis F/T sensor will certainly secure to the plastic failure of materials.

Besides being able to determine the structural integrity of the sensor, virtual prototyping simulation can illustrate the strain as an input in the measurement of force/torque using strain gauge. In addition, the placement of strain gauge on the structure can easily be known to get a good measurement of strain which is experienced during the tension and compression. Fig. 6 shows the simulation results of the strain distribution on the structure of the six-axis F/T sensor (deformation scale 120: 1) for the following loading: (a) F_x = 2000 N, (b) F_y = 2000 N, (c) F_z = 2000 N, (d) M_x = 80 Nm, (e) M_y = 80 Nm, and (f) M_z = 80 Nm. In general, the distribution of strain that occurs on the cross beam has the tension and compression, where the resistance of strain gauge in tension will increase otherwise will decrease in compression. These results are appropriate with the ideal design of a six-axis F/T sensor. By applying the same loading in the reverse direction (negative), the strain for the negative direction will be known. Then to predict a linearity and cross coupling error, each force and moment is applied stepwise by dividing the whole load range into ten increments. For example, three axial forces (F_x, $F_y$and F_z) were applied from -2000 N to 2000 N at increments of 400 N. Loads for moments (M_x, M_y and M_z) were applied from -80 Nm to 80 Nm at increments of 16 Nm.

Fig. 7 shows the simulation result of loading for pure forces and moments. All the strain

responses show excellent linearity, which indicates that the strain gauge locations are well assigned for the applied load ranges.

The maximum strain output and cross coupling error of the six-axis F/T sensor are shown in Table 2. There are two large cross coupling errors compared to the others: (CC) 15 of −1.67% and (CC)24 of 1.24%. Although there are higher strain outputs in other components, their cross coupling errors are within 1.67% at most, which is relatively small compared to the principal coupling error. Therefore, the design of six-axis F/T sensor using virtual prototyping technique is able to show satisfactory results and match expectations to provide a guideline for the design of multi-axis F/T sensors that can significantly reduce the cross coupling errors.

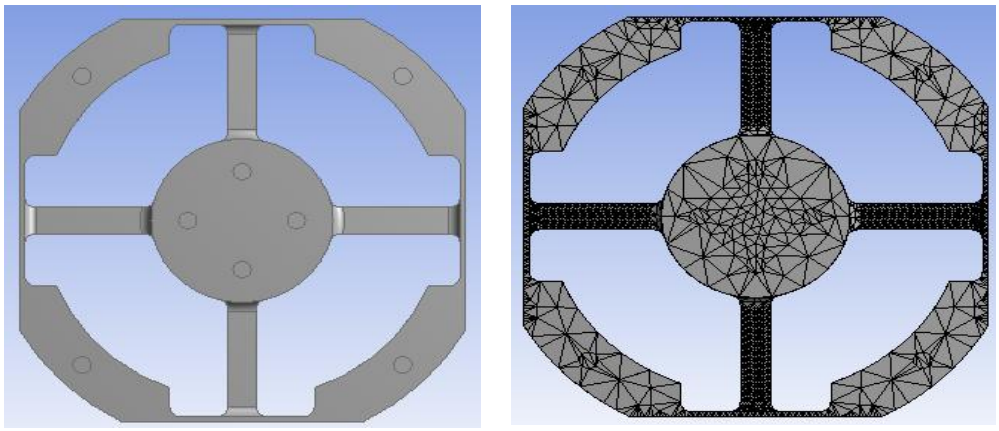

(a) **(b)**

Fig. 3(a). Geometric modelling result and (b) meshing

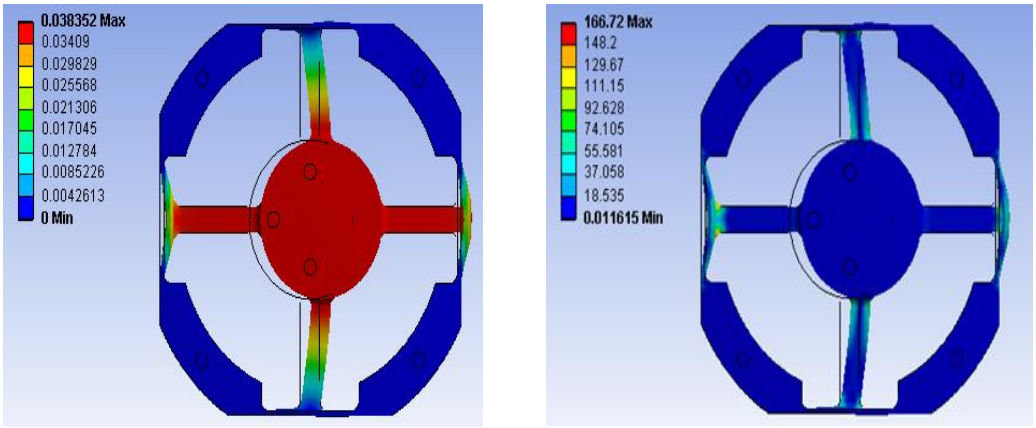

(a) **(b)**

Fig. 4(a). Deformation due to F_x(mm), (b) Equivalent stress (MPa)

Table 1. Results of deformation and integrity of sensor structure

Result	F_x	F_y	F_z	M_x	M_y	M_z
Deformation (mm)	0.038	0.038	0.081	0.083	0.082	0.029
Stress (MPa)	166.72	165.66	204.52	307.30	300.74	165.14
Safety factor	2.82	3.00	2.30	1.53	1.56	2.85

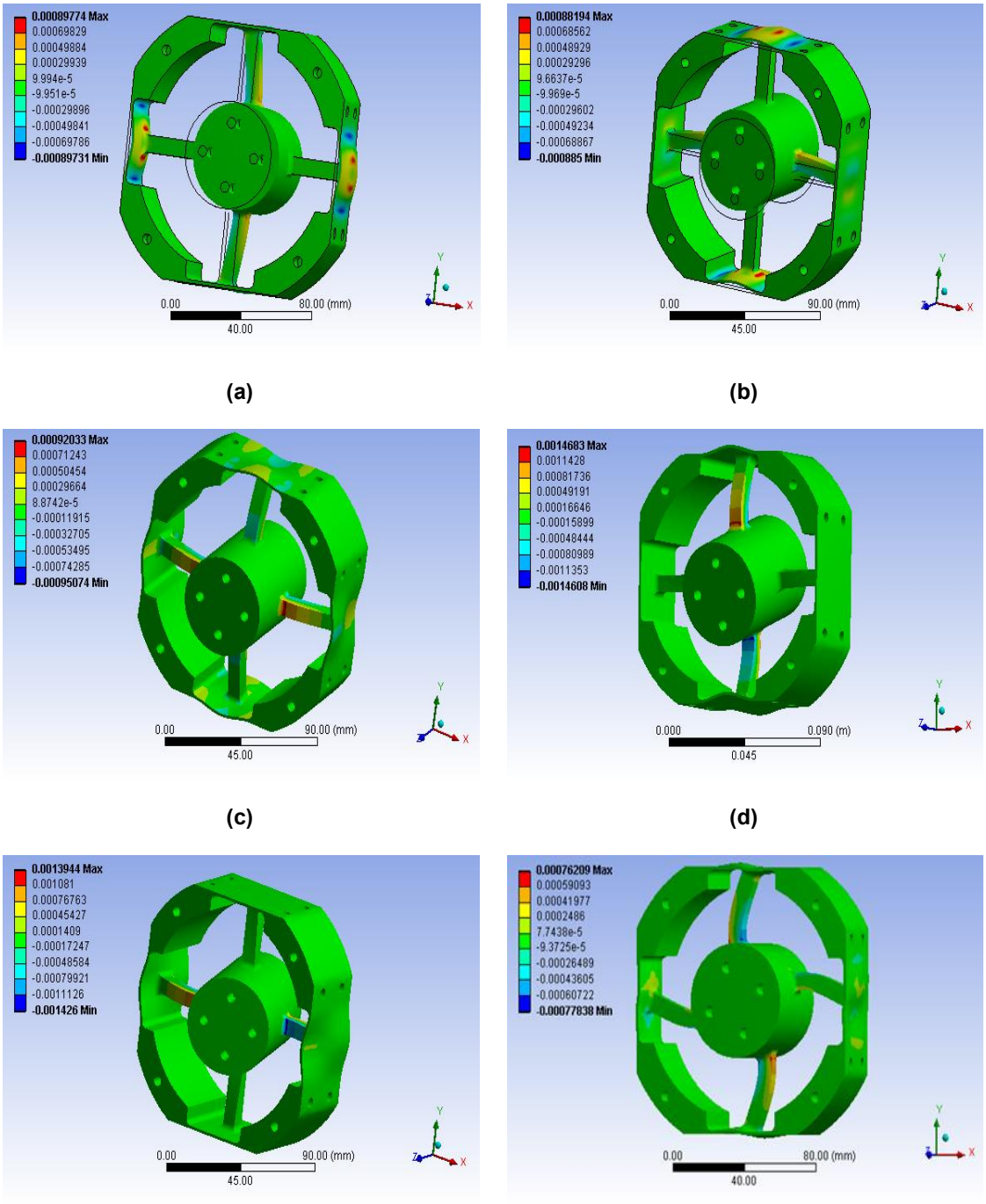

Fig. 5. FEM results under each individual force and moment: (a) F_x = 2000 N, (b) F_y = 2000 N, (c) F_z = 2000 N, (d)M_x = 80 Nm, (e)M_y = 80 Nm, (f)M_z = 80 Nm

Table 2. Simulation results of strain output (μm/m) and cross coupling error (%)

Bridge circuit	Fx=2000N		Fy=2000N		Fz=2000N		Mx=80Nm		My=80Nm		Mz=80Nm	
	Sij (μm/m)	Ccij (%)	Sij (μm/m)	Ccij (%)	Sij (μm/m)	Ccij (%)	Sij (μm/m)	Ccij (%)	Sij (μm/m)	Ccij (%)	Sij (μm/m)	Ccij (%)
SFx	293.01	-	0.40	0.14	0.26	0.04	0.55	0.09	-5.56	-0.91	-0.10	-0.03
SFy	-0.75	-0.26	297.86	-	-0.51	-0.08	4.58	0.75	0.15	0.02	0.73	0.25
SFz	0.03	0.01	-0.51	-0.17	629.48	-	-0.31	-0.05	-0.29	-0.05	0.18	0.06
SMx	-0.21	-0.07	3.68	1.24	0.13	0.02	614.16	-	-0.07	-0.01	-0.10	-0.03
SMy	-4.89	-1.67	0.39	0.13	0.15	0.02	-0.12	-0.02	613.39	-	-0.09	-0.03
SMz	-0.24	-0.08	-0.28	-0.09	-0.66	-0.10	-1.66	-0.27	0.59	0.10	291.03	-

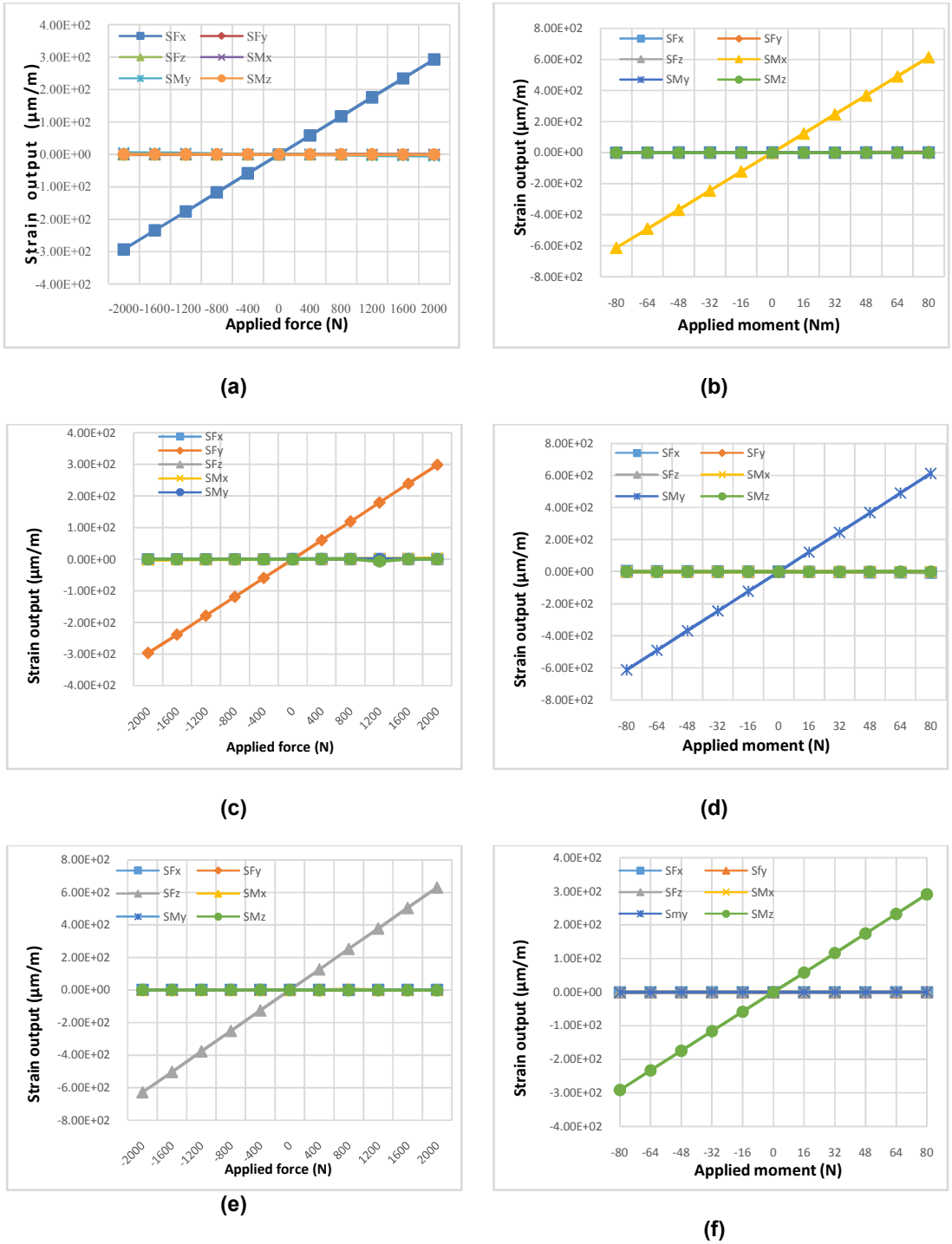

Fig. 6. Simulation results of applied forces and moments for: (a) F_x, (b) F_y, (c) F_z, (d) M_x, (e) M_y, (f) M_z

4. CONCLUSION

The structural design of the six-axis F/T sensor using virtual prototyping technique based on the finite element is capable of displaying the 3D detailed results in each segment of the sensor, Therefore it can be used as a reference in the development of physical prototypes. Based on the structural integrity evaluation of the sensor, the maximum equivalent stress occurs in M_x loading of 307.30 MPa, however the minimum safety factor is still 53% greater than the yield strength of the material, therefore the structure of the sensor will certainly secure to the plastic failure of materials because it is still in the area of elastic material. Then based on the simulation results of the strain, the highest cross-coupling errors is -1.67% which is relatively small compared to the principal coupling error. Therefore, the design of six-axis F/T sensor using virtual prototyping technique is able to show satisfactory results and match expectations to provide a guideline for the design of multi-axis F/T sensors that can significantly reduce the cross coupling errors.

COMPETING INTERESTS

The author would like to thank to the Head of Technical Implementation Unit for Instrumentation Development, Indonesian Institute of Sciences which has provided a financial support through LIPI research thematic in 2014 (No. 07901450196018). Moreover thanks to the Head of Research Center for Power and Mechatronics, Indonesian Institute of Sciences, for facilitating the finite element simulation using ANSYS.

REFERENCES

1. Yi Lu, Liwei Chen, Peng Wang, Bing Zhang, Yong Sheng Zhao, Bo Hu. Statics and stiffness analysis of a novel six-component force/torque sensor with 3-RPPS compliant parallel structure. Mechanism and Machine Theory. 2013;62:99-111.
2. Paul Schumacher, Musa Jouaneh. A force sensing tool for disassembly operations. Robotics and Computer-Integrated Manufacturing. 2014;30:206–217.
3. Yasuhiro Kakinuma, Keisuke Igarashi, Seiichiro Katsura, Tojiro Aoyama. Development of 5-axis polishing machine capable of simultaneous trajectory posture and force control. *CIRP* Annals - Manufacturing Technology. 2013;62:379–382.
4. Peter Bakia, Gabor Szekelya, Gabor Kosab. Design and characterization of a novel, robust, tri-axial force sensor. Sensors and Actuators. 2013;192:101–110.
5. Brookhuisa RA, Lammerinka TSJ, Wiegerinka RJ, de Boera MJ, Elwenspoeka MC. 3D force sensor for biomechanical applications. Sensors and Actuators. 2012;182:28– 33.
6. Esteveza P, Banka JM, Portaa M, Weib J, Sarrob PM, Tichema M, Staufera U. 6 DOF force and torque sensor for micro-manipulation applications. Sensors and Actuators. 2012;186:86– 93.
7. Demetropoulosa CK, Morgan CR, Sengupta DK, Herkowitz HN. Development of a 4-axis load cell used for lumbar interbody load measurements. Medical Engineering & Physics. 2009;31:846–851.
8. Ben Mitchell, John Koo, IulianIordachita MD, Peter Kazanzides, Ankur Kapoor, James Handa, Gregory Hager MD, Russell Taylor. Development and application of a new steady-hand manipulator for retinal surgery. IEEE international conference on robotics and automation, Roma, Italy. 2007;623-629. 10-14 April 2007.
9. Ma Yingkun, Xie Shilin, Zhang Xinong, Luo Yajun. Hybrid calibration method for six-component force/torque transducers of wind tunnel balance based on support vector machines. Chinese Journal of Aeronautics. 2013;26:554–562.
10. Qiaokang Liang, Dan Zhang, Quanjun Song, Yunjian Ge, Huibin Cao, Yu Ge. Design and fabrication of a six-dimensional wrist force/torque sensor based on E-type membranes compared to cross beams. Measurement . 2010;43:1702–1719.
11. Yulei Hou, Daxing Zeng, Jiantao Yao, Kaijia Kang, Ling Lu, Yongsheng Zhao. Optimal design of a hyperstatic Stewart platform-based force/torque sensor with genetic algorithms. Mechatronics. 2009;19: 199–204.
12. Zhijun Wang, Jiantao Yao, Yundou Xu, Yongsheng Zhao. Hyperstatic analysis of a fully pre-stressed six-axis force/torque sensor. Mechanism and Machine Theory. 2012;57:84-94.
13. Min Kyung Kang, Soobum Lee, Jung-Hoon Kim. Shape optimization of a mechanically decoupled six-axis force/torque sensor. Sensors and Actuators. 2014;209:41-51.

14. Ying-jun Li, Gui-cong Wang, Dong Zhao, Xuan Sun, Qing-hua Fang. Research on a novel parallel spoke piezoelectric 6-DOF heavy force/torque sensor. Mechanical Systems and Signal Processing. 2013;36:152–167.
15. Zhanga G, Zhoua N. Study on Integrated Design Method for Series Traction Mechanism of Heavy Machinery Based on Virtual Prototyping. Physics Procedia. 2012;25:2-7.
16. H Li, Chan NKY, Huang T, Skitmore M, Yang J. Virtual prototyping for planning bridge construction. Automation in Construction. 2012;27:1–10.
17. Wong JKW, Li H, Wang H, Huang T, Luo E, Li V. Toward low-carbon construction processes: the visualisation of predicted emission via virtual prototyping technology. Automation in Construction. 2013;33:72–78.
18. Morenilla AJ, Romero JLS, Perez FS. Augmented and Virtual Reality techniques for footwear. Computers in Industry. 2013;64:1371–1382.
19. Berti G, Monti M. A virtual prototyping environment for a robust design of an injection mouldingprocess. Computers and Chemical Engineering. 2013;54:159–169.
20. Liu GR, Quek SS. The Finite Element Method: A Practical Course, *Oxford:* Butterworth-Heinemann, Elsevier Science Ltd.; 2003.
21. Zienkiewicz OC, Taylor RL. The finite element method. Fifth Edition Volume 1: The basis, Oxford: Butterworth-Heinemann, Elsevier Science Ltd.; 2000.

Peer-review history:
The peer review history for this paper can be accessed here:
http://www.sciencedomain.org/review-history.php?iid=748&id=22&aid=7195